RSC Advances

PAPER

View Article Online
View Journal | View Issue

Check for updates

Cite this: *RSC Adv.*, 2026, **16**, 11442

Sustainable leaching of mixed LIB waste cathode employing a deep eutectic solvent composed of L-proline and lactic acid

Pratyasha Panda and Sujata Mishra *

The rapidly increasing consumption of lithium-ion batteries (LIBs), coupled with the growing volume of end-of-life batteries, underscores the urgent need for sustainable and environmentally benign recycling technologies. While deep eutectic solvents (DESs) have emerged as promising green alternatives to traditional mineral acids and organic solvents, the use of amino acid-based DESs for metal recovery from LIB waste remains largely unexplored. This study addresses this gap by developing a novel L-proline–lactic acid DES blended with 30% water specifically designed for efficient leaching of lithium, cobalt, and nickel from spent LIB cathode materials. The synergistic interaction between L-proline and lactic acid creates a unique hydrogen-bonding network that enhances metal dissolution, marking a significant advancement over conventional DES formulations. Response Surface Methodology (RSM) was employed to systematically assess and optimize the effects of temperature, leaching time, and stirring speed, leading to remarkably high leaching efficiencies under mild conditions. Experimental findings recorded leaching efficiencies of 98.32% Li, 100% Co, 99.07% Ni and, 85.63% Fe, with minimal dissolution of Mn under optimized conditions, suggesting the selectivity of the DES for Li, Co, Ni and Fe over Mn. This indicates the superior performance of amino acid-based DESs. Kinetic modelling further revealed that the leaching follows a chemical reaction-controlled mechanism, confirming direct chemical interaction between metal ions and the DES. Overall, this study showcases an innovative and environmentally friendly DES-water system that significantly achieves sustainability, efficiency, and mechanistic comprehension of lithium-ion battery recycling.

Received 3rd December 2025
Accepted 20th February 2026

DOI: 10.1039/d5ra09345g

rsc.li/rsc-advances

Open Access Article. Published on 27 February 2026. Downloaded on 5/24/2026 11:28:39 AM.
This article is licensed under a Creative Commons Attribution-NonCommercial 3.0 Unported Licence.

Introduction

Lithium ion batteries (LIBs) have become indispensable in modern technology, powering a wide array of applications from consumer electronics to electric vehicles (EVs) and renewable energy storage systems. Their high energy density, lightweight design, and long cycle life have positioned them as the preferred energy storage solution in the transition towards a more sustainable and electrified future.[1–3] The global demand for lithium-ion batteries is experiencing unprecedented growth. In 2024, the total demand surpassed 1 terawatt-hour (TWh) for the first time, driven by record-breaking EV sales and rapid expansion in battery energy storage systems (BESS).[4] Projection indicates that the global lithium-ion battery market will reach approximately USD 115.89 billion in 2025 and is expected to grow to around USD 4720 billion by 2034, exhibiting a compound annual growth rate (CAGR) of 17.69%. This surge underscores the critical role of LIBs in achieving global decarbonization goals.[5] However, the rapid proliferation of LIBs brings forth significant environmental and resource challenges. The extraction and processing of valuable metals such as Li, Co, Ni, Mn and Fe are energy intensive and have substantial ecological footprint. The accumulations of spent batteries possess risks of hazardous waste and resource depletion. Recycling emerges as a pivotal strategy to mitigate these issues, enabling the recovery of valuable materials and reducing the reliance on resource extraction. Hydrometallurgy is often preferred over pyrometallurgy for metal recovery because it operates at lower temperatures, reducing energy consumption and greenhouse gas emissions.[6–8] It offers higher selectivity and recovery efficiency for valuable metals, generates less hazardous waste, and allows for easier control of processing conditions, making it a more environmentally friendly and economically viable option. Deep eutectic solvents (DESs) offer a greener, safer alternative to traditional organic solvents and ionic liquids due to their low toxicity, biodegradability, and ease in preparation from inexpensive, renewable components. Their tunable properties, high metal extraction efficiency, and minimal environmental impact make them ideal for sustainable metal recovery processes.[9–11] However, optimizing the multiple interacting factors involved in the leaching process such as temperature, time, solid-to-liquid ratio, and DES composition is

Department of Chemistry, Institute of Technical Education and Research (FET), Siksha 'O' Anusandhan Deemed to be University, Khandagiri Square, Bhubaneswar-751030, Odisha, India. E-mail: sujatamishra@soa.ac.in

© 2026 The Author(s). Published by the Royal Society of Chemistry

Open Access Article. Published on 27 February 2026. Downloaded on 5/24/2026 11:28:39 AM. This article is licensed under a Creative Commons Attribution-NonCommercial 3.0 Unported Licence.

inherently complex. Conventionally, LIBs cathodes are leached with inorganic acids (*e.g.*, H_2SO_4, HCl) or organic acids (*e.g.*, citric, oxalic), which need additional reductants (H_2O_2/Fe^{2+}) and high acid dosage, resulting in equipment corrosion and safety issues.[12–19] These systems produce high volumes of acidic wastewater and have high downstream treatment cost. Organic acids may reduce corrosiveness to some extent, but leaching rates are reduced, and solvent recovery is usually restricted. Alhashim *et al.*[20] conducted a mechanistic study on leaching transition metals from NMC(Nickel–Manganese–Cobalt oxide) and NCA(Nickel–cobalt–aluminium oxide) cathode materials using an ethylene glycol (EG) and choline chloride (ChCl) DES. The work combined experimental leaching tests with DFT calculations and found that EG helps in weakening of the metal–oxygen bond, while Cl^- ions coordinate to form chlorometalate complexes, facilitating metal dissolution. However, the process requires high temperatures (up to 180 °C) and long leaching durations, which limits its efficiency and scalability. Additionally, concerns over the high viscosity of DES at lower temperatures and limited solvent reuse were acknowledged as challenges to be addressed before industrial application. Jafari *et al.*[21] compared binary and ternary DES systems (ChCl : Urea, ChCl : EG, and ChCl : Urea : EG) for recycling spent LIB cathodes. Their ternary DES achieved higher leaching efficiencies (Li: 97%, Co: 41%, Ni: 40%, Mn: 34%) and showed reaction kinetics governed by a mixed control shrinking core model. Yet, a limitation noted was that even ternary DES required relatively high temperatures (up to 140 °C) for efficient metal recovery, and higher viscosities hampered mass transfer, making leaching times as long as 72 hours. Tang *et al.*[22] developed a novel EG: sulfosalicylic acid dihydrate (SAD) DES characterized by strong coordination ability and low viscosity, achieving remarkable extraction efficiencies (Li: 98.3%, Co: 93.5% from pure LCO) under more moderate conditions. The study revealed that interfacial chemical reaction was the rate-limiting step in the leaching kinetics. Despite its efficiency, the relatively high cost and limited availability of SAD compared to common HBDs like urea or EG, along with stability issues at elevated temperatures, posed significant limitations for scaling this system industrially. Yan *et al.*[23] addressed viscosity and recyclability issues by formulating a guanidine hydrochloride–lactic acid DES modified with ascorbic acid. This system achieved nearly 100% leaching efficiency for both $LiCoO_2$ and NCM cathodes at just 50 °C in 24 hours and maintained its properties over at least three cycles. While effective, the limitation here lay in the gradual need for re-supplementing reducing agents like ascorbic acid and the formation of by-products over cycles, which could affect DES stability and disposal protocols. Recent studies have highlighted the potential of water regulated DESs for lithium-ion battery recycling. Yang *et al.*[24] employed a ternary DES composed of betaine hydrochloride, lactic acid and water, for leaching of metals from $LiCoO_2$ resulted in 97% Co and 99% Li at 100 °C in 20 min. They apprehended that metal dissolution proceeded *via* proton-assisted M–O bond cleavage coupled with redox reactions facilitated by hydrogen bonding and electron transfer. However, the process occurs at elevated temperature and acid-assisted redox activity. This may accelerate solvent degradation and raise concerns regarding long-term solvent stability as well as recyclability. Cheng *et al.*[25] reported that ChCl–oxalic acid–H_2O DES shows high efficiency as a lixiviant, for leaching of both Li and Co from LCO at 130 °C and 2 h. Despite its high efficiency, the requirement for high operating temperature and prolonged leaching time, and changes in solvent composition, may limit energy efficiency and cyclic reuse. These reports demonstrate that while DES-water systems deliver excellent leaching performance, challenges related to thermal demand, solvent stability, and recyclability still remain, underscoring the need for optimized DES compositions and operating conditions.

From the study of the above literature, it is clear that even DESs have demonstrated considerable potential in the recycling of spent lithium-ion batteries, most studies have predominantly focused on choline chloride-based systems combined with organic acids, urea, or ethylene glycol as hydrogen bond donors. Meanwhile, the application of amino acid-based DESs remains largely unexplored, despite their inherent advantages such as biodegradability, low toxicity, natural abundance, and excellent metal-chelating abilities.

In this context, Response Surface Methodology (RSM) stands out as an ideal statistical and mathematical tool for experimental design, process optimization, and modeling of such multifactorial systems. RSM offers several advantages over traditional one-variable-at-a-time (OVAT) approaches. Firstly, it efficiently evaluates the effects of multiple process parameters and their interactions simultaneously, significantly reducing the number of required experiments.[26] This not only saves time, resources, and experimental effort but also improves the precision and reliability of the optimization process. RSM is well-suited for identifying the most influential factors and their synergistic or antagonistic effects, which is particularly valuable in complex systems like DES-mediated metal extraction, where subtle interactions can greatly influence leaching efficiencies. Therefore, applying RSM in this study ensures a systematic, comprehensive, and statistically robust optimization of the leaching process parameters, ultimately enhancing process efficiency and sustainability.[27,28]

The novelty of this study lies in the development and application of a green, L-proline–lactic acid based deep eutectic solvent blended with water for the leaching of valuable metals from cathode active materials. Proline–lactic acid DES used in our study is considered as green and sustainable due to the nature of its constituents (L-proline and lactic acid). Proline is a natural, non-toxic, and inexpensive amino acid whereas with Lactic acid (LA) is highly green and sustainable because of its synthesis through the fermentation of renewable biomass using microbes. Furthermore, in this study 30% H_2O was added to the proline–lactic acid (1 : 1) DES and water blended DES was used for leaching which reflects the green nature of the solvent. Moreover, this work uniquely integrates the use of amino acid-based DES with RSM to statistically optimize the key leaching parameters and also helps to evaluate the interaction effects among process variables which influence the leaching efficiency. This dual approach not only introduces a new class of bio-based, environmentally friendly solvents into the field of battery recycling but also reduces the consumption of

Open Access Article. Published on 27 February 2026. Downloaded on 5/24/2026 11:28:39 AM. This article is licensed under a Creative Commons Attribution-NonCommercial 3.0 Unported Licence.

chemicals and it provides a statistically robust optimization framework, advancing both the scientific understanding and practical applicability of sustainable leaching systems.

Experimental

Materials & instrumentation

L-Proline(99% purity) and lactic acid (extra pure, 90%) were procured from Merk Life Science and used in this study without further purification. The physical and chemical properties of the synthesized DES were characterized using standard analytical techniques. Density, refractive index, viscosity, and electrical conductivity were measured over the temperature range 25 °C–55 °C using a digital density meter (Randloph Research, DDM 2910; accuracy: 0.0001 g cm^{-3}, 0.03 °C), an Abbe refractometer (MA-01; ±0.0001), an Ostwald viscometer (±0.001 mPa s), and a conductivity meter (Systronics 306; range: 0.2 μS–200 mS, ±0.20 °C), respectively. Spectroscopic analysis was performed using FTIR (JASCO FT/IR-4600 LE Varian) for functional group identification. Thermal stability was evaluated *via* thermogravimetric analysis (NETZSCH STA 449 F3 Jupiter), while elemental composition was determined by ICP-OES (Thermo fisher Scientific 7600, ICAP 7000 series). Crystallinity of waste material and residue were examined by XRD (Rigaku D/max 2400, Ultima IV, Japan), and morphological as well as elemental mapping studies were conducted using FESEM (JSM-7610F) coupled with an OXFORD windowless EDS detector.

Characterization of mixed LIBs cathode powder

The pretreatment process of the mixed LIBs collected from used smart phones to obtain cathode powder is shown in Fig. 1(a). The phase composition of the mixed LIB waste cathode active material was analyzed using X-ray diffraction (XRD) in 2 theta range 10° to 80° Fig. 1(b). The diffraction pattern revealed distinct peaks corresponding to multiple crystalline phases present in the sample. Characteristic reflections of $Li_2CoMn_3O_8$ with a cubic structure were identified by matching with JCPDS no. 00-048-0261. Peaks corresponding to $LiFeO_4$ were also observed and confirmed using JCPDS no. 00-040-1499. The presence of a $Li_{1.88}(Mn_xNi_{1-x})_{1.12}O_3$ peak with a monoclinic structure was detected with JCPDS no. 00-052-0458. The identification of these phases indicates the heterogeneous composition of the spent cathode active material, comprising mixed oxide and phosphate based compounds. The particle size distribution of the cathode active material was determined (Fig. 1(c)), and the results are summarized as follows: Dv (50) was recorded at 10.785 μm, indicating that 50% of the total particle volume lies below this size. The Dv (10), Dv (90), Dv (99), and Dv (100) values were found to be 5.514 μm, 19.237 μm, 26.323 μm, and 31.053 μm, respectively. The average particle size (Dv [4,3]) of the sample was 11.647 μm. These results indicate that the waste material primarily consists of fine to medium-sized particles, with the majority of the particle volume distributed within the 5–26 μm range. This plays a crucial role in influencing the efficiency of subsequent leaching.

Fig. 2 represents the FESEM images and EDX analysis of the cathode active material. The FESEM images, captured at 1 μm, 5 μm, and 10 μm magnifications, reveal a predominantly globular morphology. The cathode material surface is covered by a hazy matrix attributed to carbon additives commonly present in cathode material. The EDX spectrum corroborates the elemental composition, identifying all characteristic elements (Fe, Ni, Mn, Co, O, and C) of the cathode material. The overall metal compositions of the mixed spent LIBs was determined by

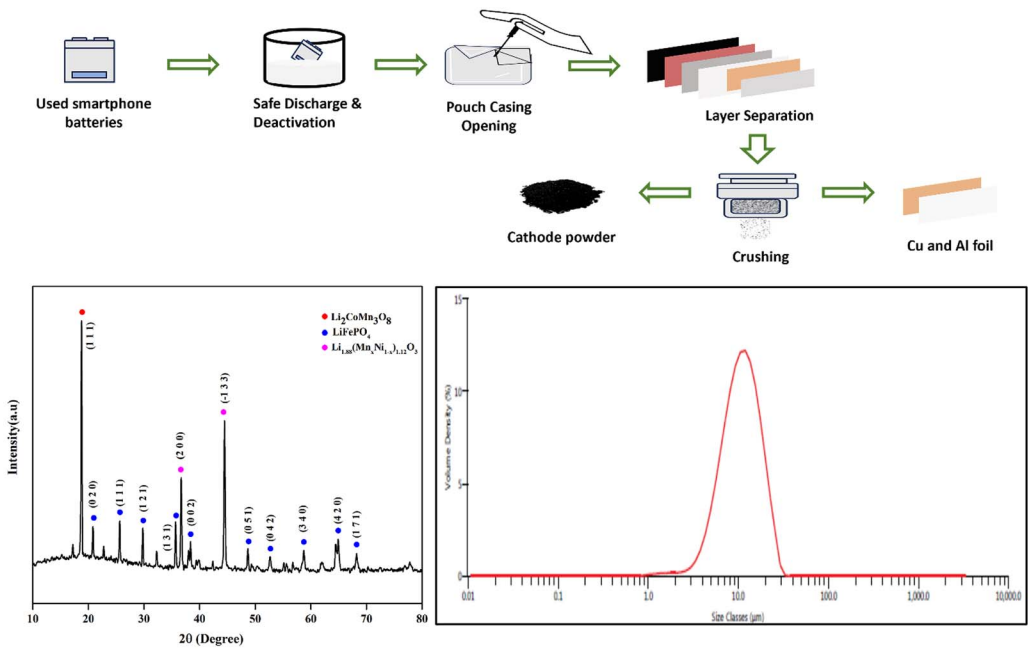

Fig. 1 (a) Schematic representation of pretreatment process (b) XRD patterns of the spent mixed LIBs with typical crystalline phases (c) particle size distributions of the spent mixed LIBs.

© 2026 The Author(s). Published by the Royal Society of Chemistry

Open Access Article. Published on 27 February 2026. Downloaded on 5/24/2026 11:28:39 AM. This article is licensed under a Creative Commons Attribution-NonCommercial 3.0 Unported Licence.

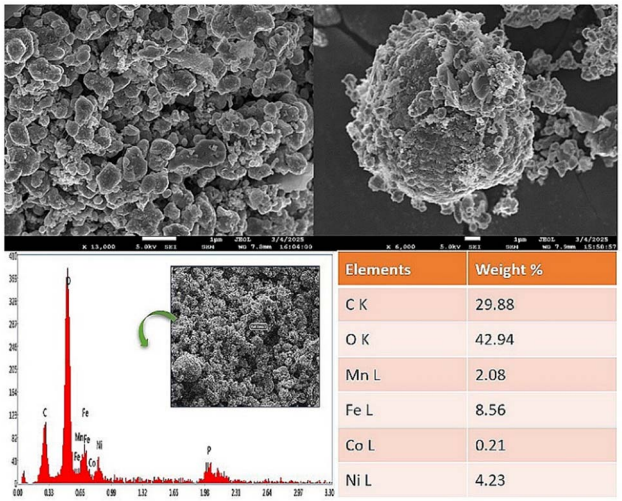

Fig. 2 SEM-EDX of spent mixed LIBs with the illustration of surface morphology and elemental analysis.

digesting the sample in aqua regia ($HCl : HNO_3 = 3 : 1$) followed by analysis using ICP-OES. The concentration of metals present in the spent mixed LIBs cathode powder listed in Table 1.

DES preparation, characterization and thermal stability

Proline : lactic acid (1 : 1) DES was formulated by mixing L-proline and lactic acid. Double distilled water (10–40% (w/w)) was added to it in order to facilitate dissolution. The mixture was subjected to constant stirring at 323.15 K. Stirring and heating were continued until a transparent and homogeneous liquid was obtained, confirming the successful formation of the DES.[29] The content of water is a key factor for the leaching behavior of DES.[30] Hammond *et al.*, reported that the structural integrity of most of the DESs is retained even when the water content reaches ~42% wt%.[31,32] Fig. 3 illustrates the structural presentation of Pro:LA DES, showing the hydrogen bonding between the components on the basis of the optimized structures for L-proline-carboxylic acid HDESs given by Maharana *et al.*[33]

The FTIR spectra of L-Proline, lactic acid, and L-Pro : LA(1 : 1) + (10–40%) H_2O DES is shown in the Fig. 4(a) and (b). The OH stretching vibrations observed at 3380.6 cm^{-1} in L-proline and 3414.35 cm^{-1} in lactic acid have been shifted to 3383.5 cm^{-1} in the DES. Similarly, N–H stretching peak of L-proline, initially observed at 3051.8 cm^{-1} was shifted to 3239.83 cm^{-1} in the DES. The CN stretching vibration of L-proline was shifted from 1447.31 cm^{-1} to 1455.03 cm^{-1} in the DES. The C=O stretching bands at 1614.13 and 1719.23 cm^{-1} in L-proline and lactic acid also got shifted to 1608.34 cm^{-1}, while the COO^- peak of L-proline exhibited a shift from 1373.07 cm^{-1} to 1397.17 cm^{-1} in

Table 1 Metals present after aqua regia digestion

Metals	Li	Co	Ni	Fe	Mn
Concentration in g L^{-1}	1.46	0.042	0.846	1.712	0.416

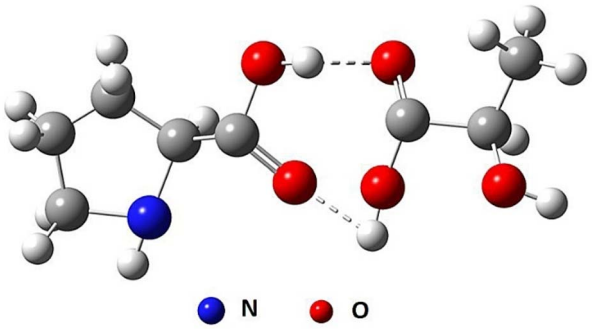

Fig. 3 Structural presentation of the L-pro:LA DES.

the DES. These characteristic peaks' shifting clearly demonstrate the establishment of an extensive H-bonding network between L-proline and lactic acid, which is responsible for the formation and stability of the DES. The broad absorption peaks observed in the range of 3400–3200 cm^{-1} in all cases correspond to the stretching vibrations of OH and NH groups. The OH peak broadening is an indication of extensive hydrogen bonding between the L-proline and lactic acid. With increase in water content, the OH stretching bands slightly shift toward higher wavenumbers from 3379.52 cm^{-1} at 10% to 3388.75 cm^{-1} at 40%, demonstrating increase in hydrogen-bonding interactions in presence of more water. The peaks observed in the range 1605–1613 cm^{-1} are attributed to the stretching vibration from C=O groups. The slight shift and changes in intensity of these peaks with increasing water content suggest alterations in orientation of H-bonding within the DES matrix. The peaks in the region of 1454–1456 cm^{-1} relate to CN stretching vibrations, whereas the peaks at 1397 cm^{-1} are associated with COO^- stretching vibrations. These observations are consistent with the known behavior of DES upon hydration, where moderate water addition facilitates molecular mobility without causing any disruption to hydrogen bonding network in eutectic mixture.

Leaching

Leaching experiments were performed in a three-neck round bottom flask fitted with a magnetic stirrer and a condenser. The

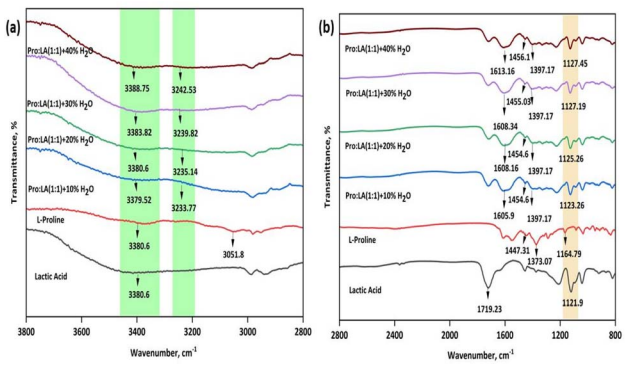

Fig. 4 FTIR spectra of lactic acid, L-proline, Pro : LA (1 : 1) + (10–40%) H_2O DES (a) 3800–2800 cm^{-1} (b) 2800–800 cm^{-1}

Open Access Article. Published on 27 February 2026. Downloaded on 5/24/2026 11:28:39 AM. This article is licensed under a Creative Commons Attribution-NonCommercial 3.0 Unported Licence.

lixiviant Pro : LA (1 : 1) + 30% H_2O DES was added to the flask containing 20 g L^{-1} cathode powder and continuous stirring was performed while maintaining the desired reaction temperature. After the required duration, the leachate was filtered off and residue if any was collected. The filtrate was analyzed to know the contents of Li, Co, Ni, Fe, and Mn using ICP-OES. The leaching efficiency of Li, Co, Ni, Fe and Mn was calculated using eqn (1).

$$L\ (\%) = \frac{(C_L \times V_L)}{(W \times C_0)} \times 100 \quad (1)$$

where, L% is the leaching efficiency in percentage, C_L is the concentration of the metals in g L^{-1} after leaching, V_L is the total volume of the leach solution, W is the weight of mixed spent cathode material subjected to leaching and C_0 is the initial metal content.

Results and discussion

Thermo-physical properties

The physicochemical properties of the prepared Pro : LA (1 : 1) + 30% H_2O DES were systematically investigated over a temperature range of 298 K to 323 K. It was observed that the density of the DES-water was decreased from 1.1902 g cm^{-3} to 1.1012 g cm^{-3} with increasing temperature as shown in Fig. 5(a). This behaviour may be attributed to the enhanced molecular motion at elevated temperatures, which leads to enhancement in the intermolecular spaces, thereby reducing the overall density of the system.[19,34] Similarly, the refractive index values of the DES exhibited a decreasing trend from 1.462 to 1.458 with rise in temperature (Fig. 5(b)). This reduction is a consequence of the diminished cohesive forces and increased molecular vibrations at higher temperatures, causing a decrease in the optical density of the medium as well as polarizability.[35,36] These temperature-dependent variations in density and refractive index reflect the thermal sensitivity of the DES and indicate significant changes in molecular interactions within the system as thermal energy increases. The density and refractive index values as function of temperature were fitted to linear and polynomial equations and the experimental values along with the calculated ones have been presented in Fig. 5. The fitting equations relating the parameters and temperature have been considered as given in our previous report.[36] Both density and refractive index data were found to be well fitted by second order polynomial equations with R^2 value of 0.9968 and 0.9977, respectively. The high R^2 values reflect good correlation between the experimental data and calculated ones.

The viscosity and electrical conductivity of the prepared DES were examined as a function of temperature in the range of 298 to 323 K. It was observed that the viscosity of the DES decreased from 50.893 to 41.538 mPa s on increasing temperature as shown in the Fig. 6(a). This behaviour can be explained by the fact that as temperature rises, the thermal energy of the system increases, which disrupts the intermolecular hydrogen bonding and weakens the cohesive forces between the DES components, thereby facilitating easier molecular movement and reducing viscosity.[37] The electrical conductivity of the DES increases with rising temperature. This enhancement in conductivity is attributed to the greater mobility of charge carriers at elevated temperatures due to reduced viscosity and enhanced molecular dynamics.[38] As temperature increases, the ionic species in the DES experience less resistance to movement, leading to improved ion transport and higher conductivity values from 5.96 to 11.231 mS m^{-1} as shown in the Fig. 6(a). Fig. 6(b) represents the Arrhenius plots of ln η(mPa s) and ln κ(mS m^{-1}) as a function of 1000/T(K^{-1}), were used to evaluate the activation energies for viscous flow and conduction. The activation energy for viscous flow, calculated using the Arrhenius equation, was found to be 6.718 kJ mol^{-1}, indicating a moderate energy barrier for the viscous motion of DES molecules.[36] The activation energy for electrical conductivity determined from the Arrhenius plot was found to be 21.661 kJ mol^{-1}. This means that the carriers can overcome this energy barrier and become mobile since they have access to greater thermal energy at higher temperature.

Preliminary experiments

The rate and extent of leaching are influenced by numerous factors, comprising the nature of the solvent, solid particle size, temperature, leaching time and solid porosity. The influence of water addition on dissolving metal values from LIB cathode was assessed using DES having different water content (10–40%) in the leaching profile is shown in Fig. 7. The efficiency of leaching of the metals was noted to improve remarkably with increase in the water content up to 30%. This enhancement may be ascribed to the decrease in viscosity of the DES-water combination, which evidently leads to a faster diffusion and mass transfer kinetics.[39] Beyond this, a slight decline in efficiency was observed, indicating that excessive dilution disrupting the H-

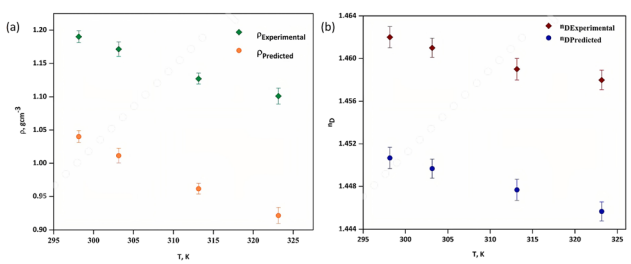

Fig. 5 Variation of experimental and predicted (a) ρ (g cm^{-3}), and (b) n_D as a function of T(K).

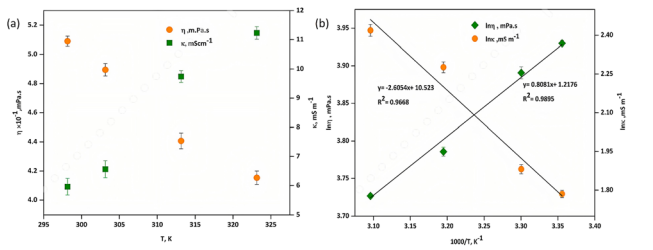

Fig. 6 (a) η(mPa s) and κ(mS m^{-1}) as a function of temperature, (b) arrhenius plots of ln η(mPa s) and ln κ(mS m^{-1}) as a function of 1000/T(K^{-1}).

© 2026 The Author(s). Published by the Royal Society of Chemistry

Open Access Article. Published on 27 February 2026. Downloaded on 5/24/2026 11:28:39 AM. This article is licensed under a Creative Commons Attribution-NonCommercial 3.0 Unported Licence.

bond network of the DES, reducing its leaching capability. The structural and physicochemical studies of different DESs reported that hydration affects their hydrogen-bonding network strongly but non-linearly. Neutron scattering as well as EPSR analyses revealed that water firstly integrates into the DES structure and is preferentially organized around HBA, allowing the DES structure to persist up to relatively high hydration levels.[40] Within this regime, water reduces the viscosity and enhances the ionic mobility while preserving the cooperative hydrogen bonding between the DES components which is important for effective metal dissolution. In the present investigation, at low water content (10 wt%), the hydrogen bonded DES framework is largely intact, but the system remains highly viscous, which restricts mass transfer and slows leaching kinetics. At higher water content (40 wt%), water self-association becomes increasingly dominant, leading to dispersion of DES aggregates and progressive loss of the defining eutectic features. Although some DES hydrogen bonding may remain, the solvent increasingly behaves as a water-rich medium, resulting in weaker metal-DES interactions and reduced the leaching efficiency. Therefore, 30 wt% water represents an optimal content where sufficient hydration improves fluidity and transport properties without significant disruption of the DES hydrogen-bonding network, leading to superior leaching performance. Thus, in this work DES with 30% water was taken to carry out all further experiments.

The thermal stability of the Pro : LA (1 : 1) + 30% H_2O was examined with the help of TG-DTA studies as represented in Fig. 8. The TGA curve indicated an initial weight loss of 18.80% occurring between 313–333 K, which is attributed to the evaporation of moisture and physically adsorbed water within the DES. As the temperature increased, a noticeable endothermic peak appeared at 413.3 K in the DTA curve, marking the onset of the primary decomposition stage. The most significant mass loss was recorded between 430 and 573 K, where approximately 79.7% of the total sample mass was lost, indicating extensive thermal degradation of the DES components. These observations highlight the thermal behavior and stability limits of the system, offering valuable insights for optimizing operating temperature to be used in thermally driven applications such as leaching.

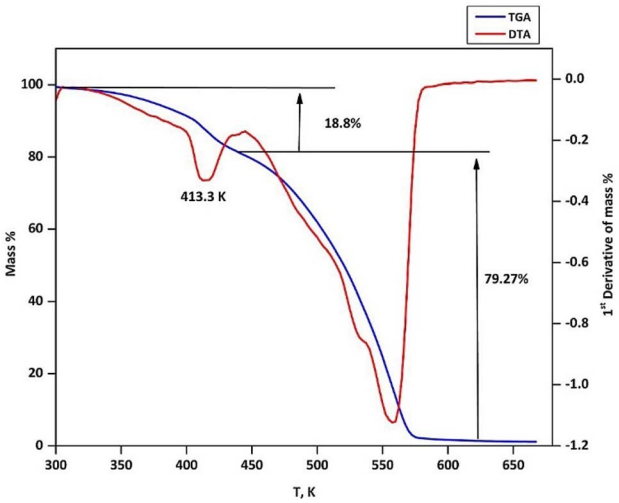

Fig. 8 TG-DTA of the Pro : LA (1 : 1) + 30% H_2O DES demonstrating mass loss and heat flow corresponding to thermal stability and decomposition peaks.

Three important parameters such as temperature, S/L ratio and leaching time were varied to analyze the leaching behavior of all metals present in LIB cathode waste using Pro : LA (1 : 1) + 30% H_2O as shown in the Fig. 9. An increase in temperature from 323 K to 353 K (S/L ratio = 20 g L^{-1}, time = 60 min)shows positive impact on leaching efficiencies for Li (59.63 to 96.52%), Co (64.77 to 97.35%), Ni (53.66 to 95.63%), Fe (51.47 to 40.58%) and Mn (19.37 to 40.58%) as displayed in Fig. 9(a). As metal leaching methods are endothermic in nature, the high reaction temperatures produce thermodynamically favourable conditions in the course of leaching.[41] The influence of variation of S/L ratio from 10 to 50 g L^{-1}(Temp. = 353 K and time = 60 min) on leaching efficiency is shown in Fig. 9(b). Leaching efficiency in cases of all metals increases up to 20 g L^{-1} (96.52% for Li,

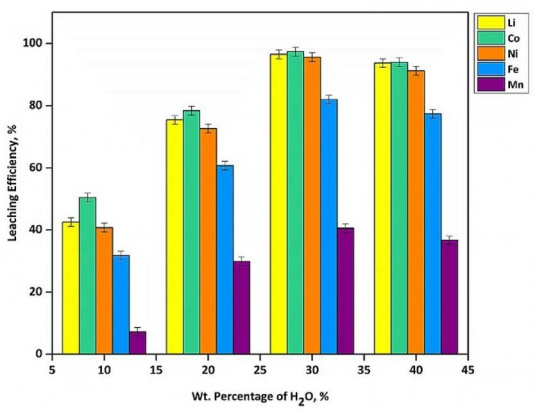

Fig. 7 Leaching efficiency of metal values from cathode waste *versus* weight percent of water in Pro : LA (1 : 1) DES.

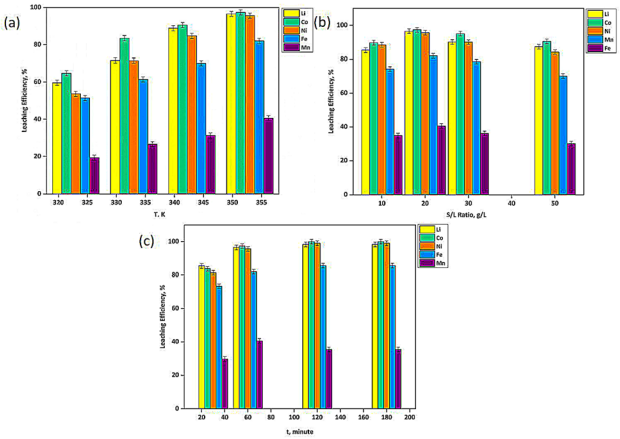

Fig. 9 Effect of different process parameters on the leaching efficiency of Li, Co, Ni, Fe and, Mn from mixed spent LIBs, (a) effect of temperature, (b) effect of solid-to-liquid ratio, and (c) effect of leaching time.

Open Access Article. Published on 27 February 2026. Downloaded on 5/24/2026 11:28:39 AM. This article is licensed under a Creative Commons Attribution-NonCommercial 3.0 Unported Licence.

Table 2 Summary of the selected input variables, their corresponding experimental levels, and associated standard deviation values

Name	Units	Minimum	Maximum	Coded low	Coded high	Mean	Std. dev.
Time(A)	minute	39.55	140.45	−1 ↔ 60	+1 ↔ 120	90	25.43
Temperature(B)	kelvin	299.36	366.64	−1 ↔ 313	+1 ↔ 353	333	16.96
Stirring speed(C)	rpm	497.73	1002.27	−1 ↔ 600	+1 ↔ 900	750	127.17

97.35% for Co, 95.63% for Ni, 81.98% for Fe, and 40.58% for Mn) due to the better availability of lixiviant per unit mass of solid at lower S/L ratio. However, at higher S/L ratios (30–50 g L^{-1}), a decline in efficiency was observed, possibly due to insufficient solvent availability and mass transfer limitations. The effect of leaching time variation from 30 to 180 min (S/L ratio = 20 g L^{-1}, Temp. = 353 K) on leaching efficiency of metals has been depicted in Fig. 9(c). A rapid increase in leaching efficiency was noted up to 120 min, with 98.32% for Li, 100% for Co, 99.07% for Ni, 85.63% for Fe, and 35.42% for Mn. Further increase in leaching time after 120 minute did not result in any improvement in leaching efficiency, indicating that equilibrium conditions was reached at 120 min.

Design of experiment

To assess the influence of various operational parameters on the leaching efficiencies of Li, Mn, Fe, Co and Ni from spent lithium-ion battery (LIB) cathodes, a design of experiments (DoE) approach was employed using RSM *via* Central Composite Design (CCD). RSM is a powerful statistical and mathematical technique used for modelling and analysing problems where several independent variables influence a response.[42,43] CCD, a common and effective design within RSM, was selected for its efficiency in fitting a second order (quadratic) model and its ability to evaluate the interactive effects between variables with a minimal number of experiments. The design and statistical analysis was done using the Design Expert Software-12(Start-Ease). Three key leaching parameters were selected as independent variables: leaching time (minute), temperature (Kelvin) and, stirring speed (rpm). Each variable was studied at five levels using coded values; ±1 for factorial points, 0 for centre points, and $\pm\alpha$ (=1.6817) for axial points. A total of 20 points, and 6 replicates at the centre to estimate experimental error and ensure model reliability. The design aimed to generate an empirical model using a second-degree polynomial equation, incorporating linear, interaction, and quadratic-terms. Analysis of variance (ANOVA) was used to evaluate the statistical significance of the model and the effects of individual variables and their interactions on leaching efficiency.[44] The experimental design was randomised to minimise bias and reduce the influence of uncontrolled factors. The model developed through RSM enabled the prediction and optimization of process parameters for obtaining maximum leaching efficiency. This approach not only provided insight into the effect of each factor but also identified the optimal conditions for efficient leaching, thus demonstrating the practical utility of RSM-CCD in leaching beneficiation processes. The methodology significantly reduced experimental work while improving understanding the process and its performance. Regression analysis of the experimental data, along with the generation of response surface and contour plots at

Table 3 Experimental runs with leaching efficiencies of metals present in cathode materials under different conditions

	Factor 1	Factor 2	Factor 3	Leaching efficiency (%)				
Run	Time	Temperature (K)	Stirring speed (rpm)	Li	Co	Ni	Fe	Mn
1	60	313	900	48.67	50.34	48.53	37.43	15.67
2	90	333	750	83.63	80.63	78.68	68.52	23.47
3	90	299.4	750	27.26	33.68	31.69	14.38	0
4	120	353	900	98.32	100	99.07	85.63	35.42
5	120	313	600	45.87	47.96	46.96	33.64	13.74
6	90	333	497.7	65.37	69.74	68.47	59.37	19.35
7	60	353	600	90.22	91.74	91.44	75.38	35.83
8	60	353	900	96.52	97.35	95.63	81.98	40.58
9	90	333	750	78.47	72.68	83.53	63.27	25.39
10	90	333	750	76.84	82.78	85.64	72.14	31.45
11	90	333	750	84.33	76.32	76.25	70.41	22.77
12	39.5	333	750	62.94	67.39	65.98	55.28	23.68
13	60	313	600	42.65	45.38	43.85	29.78	10.05
14	90	333	750	75.96	84.69	76.44	65.32	28.37
15	90	333	1002.3	85.41	87.52	86.34	73.07	32.47
16	90	333	750	73.69	74.68	82.05	70.84	20.88
17	120	353	600	93.74	95.85	93.25	78.47	37.94
18	90	366.6	750	97.12	99.02	98.37	83.96	39.68
19	120	313	900	52.6	54.37	56.77	42.84	17.09
20	140.4	333	750	86.44	88.06	87.37	71.85	33.24

© 2026 The Author(s). Published by the Royal Society of Chemistry

Open Access Article. Published on 27 February 2026. Downloaded on 5/24/2026 11:28:39 AM. This article is licensed under a Creative Commons Attribution-NonCommercial 3.0 Unported Licence.

Table 4 Statistical analysis parameters obtained from ANOVA, including R^2, adjusted R^2, predicted R^2, adequate precision, standard deviation, mean, and coefficient of variation for leaching model

Source	Li	Co	Ni	Fe	Mn
R^2	0.9690	0.9647	0.9749	0.9868	0.9428
Adjusted R^2	0.9411	0.9330	0.9523	0.9750	0.8913
Predicted R^2	0.8348	0.8273	0.8713	0.9488	0.7765
Adeq precision	21.4388	20.2725	23.7895	33.4327	15.6730
Std. dev.	4.99	5.10	4.33	3.15	3.55
Mean	73.30	75.01	74.82	61.68	25.35
C. V.%	6.81	6.80	5.79	5.11	14.02

optimised conditions were performed. The statistical validity of the model was confirmed through the *F*-test, while the accuracy of the model and significance were determined based on the coefficient of determination (R^2) and *p* values at a 95% confidence level. The selected input variables along with their experiment levels and standard deviation values are represented in Table 2. The details of the experimental set up along with the percentage leaching efficiencies of the mixed spent cathode materials under different conditions are presented as Table 3.

Fitting of the model through ANOVA and optimization of process

The leaching efficiencies of Li, Co, Ni, Mn, and Fe as response were analyzed using Analysis of Variance (ANOVA). The results confirmed that quadratic polynomial model provides the best fit in all cases. The significance of the model was established by taking into account the high *F*-values and low *p*-values ($p < 0.05$), indicating that the model terms were statistically significant at a 95% confidence level. The lack-of-fit test was found to be non-significant, confirming the adequacy of the model to represent the experimental data. The strength of the model was further validated by high values of R^2, adjusted R^2, and predicted R^2, demonstrating that the quadratic model was suitable for accurately describing and predicting the leaching behavior of the metals under study represented in Table 4. Based on the ANOVA results, the regression model describing the leaching behaviour of Li, Co, Ni, Fe, and Mn in the Pro : LA (1 : 1) + 30% H_2O are presented in the following eqn (2)–(6). The leaching efficiency of metals including Li, Co, Ni, Mn and Fe was investigated by altering three critical parameters: time, temperature, and stirring speed. The results demonstrate that temperature is crucial in improving leaching in improving leaching efficiency. At 353 K and 120 minutes (run 4), the leaching efficiencies for Li, Co and Ni were remarkably high 98.32%, 100% and 99.07%, respectively. This is probably attributed to higher molecular motion at elevated temperature, which accelerates the dissolution of metal ions into the leaching solution by overcoming the activation energy barrier.

$$\%\,L(\mathrm{Li}) = +78.79 + 3.81 \times A + 22.44 \times B + 4.2 \times C - 0.2288 \times AB - 0.1263 \times AC - 0.2338 \times BC - 1.29 \times A^2 - 5.71 \times B^2 - 1.04 \times C^2 \quad (2)$$

$$\%\,L(\mathrm{Co}) = +78.6 + 3.52 \times A + 21.73 \times B + 3.74 \times C + 0.0187 \times AB - 0.0013 \times AC - 0.2013 \times BC - 0.551 \times A^2 - 4.57 \times B^2 - 0.231 \times C^2 \quad (3)$$

$$\%\,L(\mathrm{Ni}) = +80.45 + 3.85 \times A + 21.63 \times B + 3.99 \times C - 0.7625 \times AB + 0.845 \times AC - 0.56 \times BC - 1.47 \times A^2 - 5.58 \times B^2 - 1.21 \times C^2 \quad (4)$$

$$\%\,L(\mathrm{Fe}) = +68.45 + 3.21 \times A + 21.59 \times B + 3.93 \times C - 0.3162 \times AB + 0.2637 \times AC - 0.3862 \times BC - 1.92 \times A^2 - 7.01 \times B^2 - 0.9826 \times C^2 \quad (5)$$

$$\%\,L(\mathrm{Mn}) = +25.35 + 1.33 \times A + 11.71 \times B + 2.44 \times C - 1.02 \times AB - 1.19 \times AC - 0.8425 \times BC + 1.32 \times A^2 - 1.73 \times B^2 + 0.4151 \times C^2 \quad (6)$$

Elevating stirring speed from 600 rpm to 900 rpm, the leaching efficiency was enhanced due to more mass transfer between cathode powder and the DES. This enhanced interaction facilitates more efficient solvent infiltration into the solid black mass, thereby promoting metal ion release. Beyond a specific threshold (run 15), the enhancement in leaching efficiency was minimal, indicating a limitation to the advantages of agitation, presumably due to saturation of the DES medium. Leaching duration was another pivotal factor. Extended leaching time facilitated metal extraction, evidenced by 120 minute runs producing superior results compared to 60 or 90 minute intervals. This is because leaching is a time dependent process of diffusion and reaction, in which adequate contact time guarantees that the interaction between the leachant and the cathode powder attains equilibrium. The plots of predicted *versus* actual values of leaching efficiencies (Fig. 10) demonstrate good agreement between the experimental data and the model outcomes for all the five metals (Li, Co, Ni, Fe, and Mn). The close alignment of the data points along the diagonal line indicates the reliability of the developed model in accurate estimation of leaching efficiencies. Based on RSM-CCD optimization results by ANOVA analysis (Table S1 given in supporting information), temperature (p value < 0.0001) has emerged as the most influential parameter in leaching study of all metals, which is attributed to its contribution pronounced influence on DES viscosity reduction enhancing mass transfer as well as leaching kinetics. Stirring speed is the second important parameter (p values = 0.0111 for Li, 0.0220 for Co, 0.0067 for Ni, 0.001 for Fe and 0.0298 for Mn). Leaching time (p values = 0.0183 for Li, 0.0287 for Co, 0.0083 for Ni, 0.0037 for Fe and 0.1974 for Mn) has the least contribution, mainly governed the extent of reaction and approach to equilibrium, with a more noticeable effect on Li than on transition metals than on Li. Based on the ANOVA results, Li exhibits the lowest overall model sensitivity ($F = 34.74$) compared to the Ni and Fe indicating relatively weaker dependence on operating parameters due to its faster dissolution kinetics and non-coordinating ability. In contrast, Co ($F = 30.39$), Ni ($F = 43.11$), Fe ($F = 83.32$). While, Mn ($F = 18.31$) shows lowest model sensitivity as it exhibited the lowest leaching efficiency among all the metals,

Open Access Article. Published on 27 February 2026. Downloaded on 5/24/2026 11:28:39 AM. This article is licensed under a Creative Commons Attribution-NonCommercial 3.0 Unported Licence.

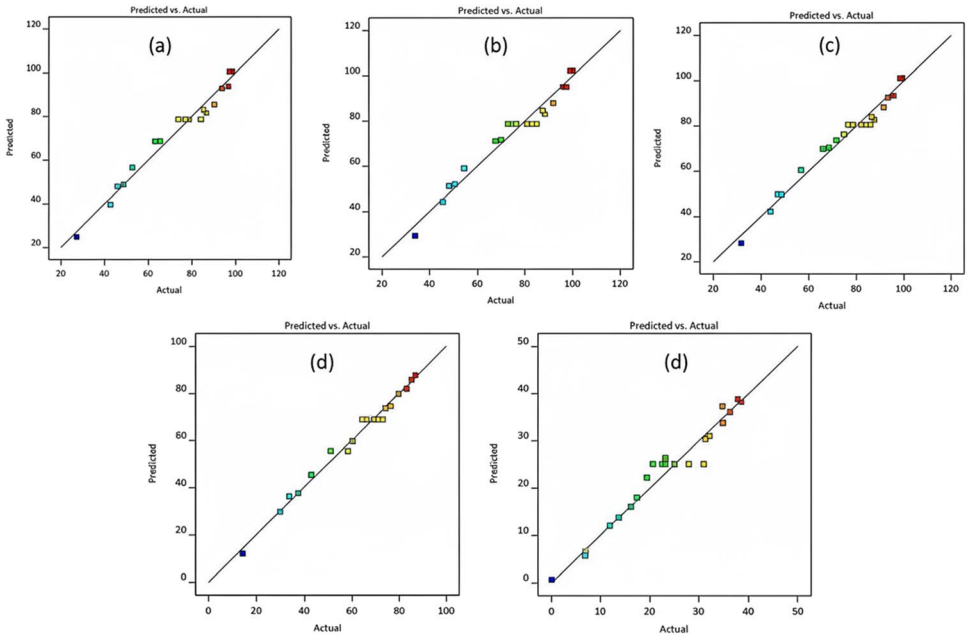

Fig. 10 Predicted *versus* actual plots for (a) Li, (b) Co, (c) Ni, (d) Fe and (e) Mn showing good agreement between experimental and model values.

confirming that transition-metal leaching is more strongly governed by temperature and coordination effects within the DES system.

In order to maximize the recovery of metals from mixed spent LIBs cathode powder using the Pro : LA (1 : 1) + 30% H_2O, the process was optimized using temperature, stirring speed and leaching duration as the primary factors. Under the optimized conditions of temperature 353 K, leaching time 120 minutes, and stirring speed of 900 rpm, the experimental leaching efficiencies were found as 98.52% for Li, 100% for Co, 99.07% for Ni, 85.63% Fe, and 35.42% for Mn. These findings are in good agreement with the predicted values using CCD, with discrepancies remaining below 5%, thereby supporting the precision of the optimization process. The results demonstrate that the selected circumstances facilitate high dissolution of Li, Co, and Ni, but Fe exhibit comparatively less leaching and Mn dissolution was lowest. Response surface plots shown in the Fig. 11–13 depict the influence of leaching time, stirring speed and temperature on the leaching efficiencies of Li, Co, Ni, Fe, and Mn.

Leaching mechanistic insights

The images of the Pro : LA (1 : 1) + 30% H_2O before and after leaching at different leaching duration are provided in Fig. 14.

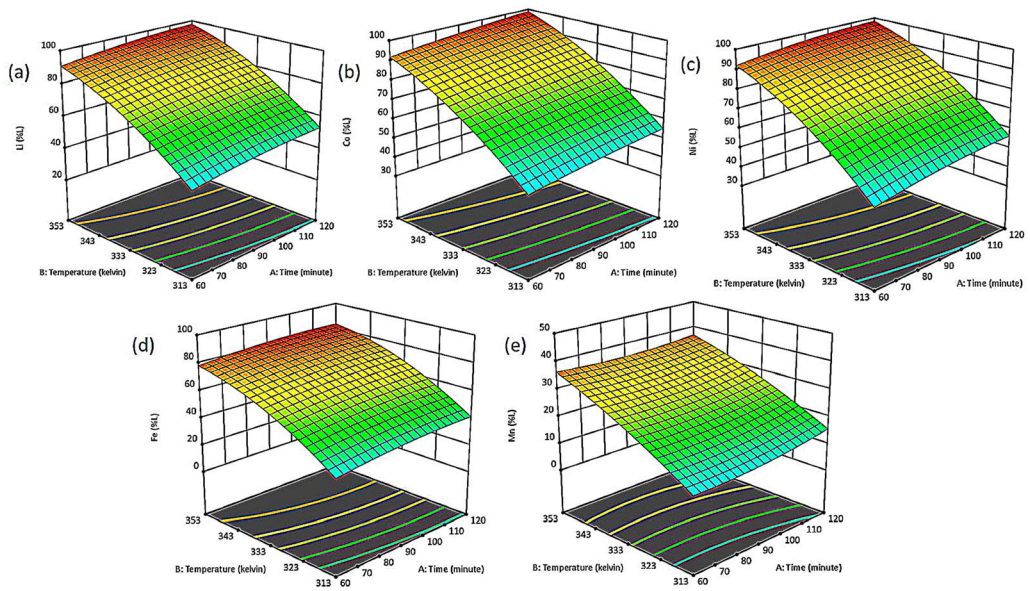

Fig. 11 Response surface plots showing the temperature and time on the leaching efficiency of (a) Li, (b) Co, (c) Ni, (d) Fe, and (e) Mn.

© 2026 The Author(s). Published by the Royal Society of Chemistry

Open Access Article. Published on 27 February 2026. Downloaded on 5/24/2026 11:28:39 AM.
This article is licensed under a Creative Commons Attribution-NonCommercial 3.0 Unported Licence.

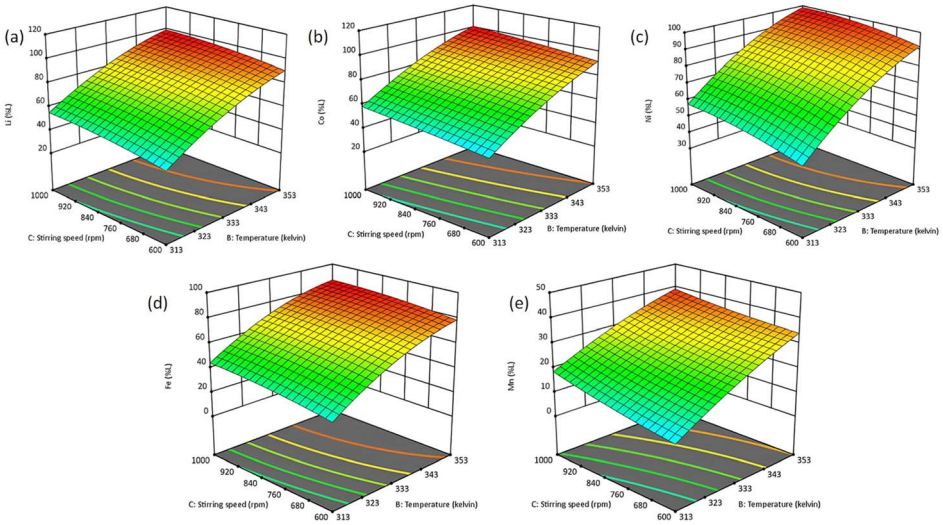

Fig. 12 Response surface plot showing the effect of stirring speed and temperature on the leaching efficiency of (a) Li, (b) Co, (c) Ni, (d) Fe, and (e) Mn.

This shows that as time increases the color of the leachate becomes more intense indicating increase in leaching percentage. The changes in physico-chemical properties and FTIR spectral characteristics provide valuable insights into the leaching mechanistic aspects of leaching of metal values from LIB cathode waste using eco-friendly amino acid based Pro : LA (1 : 1) + 30% H_2O. Leaching performance of DESs for valuable metals is closely related to their viscosity, acidity, coordination capability, and reducibility. The measured values (density, refractive index, and viscosity) displayed noticeable increase after a single leaching cycle (1.405 g cm^{-3}, 1.471, and 52.85 mPa s, against 1.1902 g cm^{-3}, 1.462 and 50.893 mPa s respectively). An increase in pH from 2.551 to 3.041 after leaching indicates proton consumption during metal dissolution. These changes are irreversible, and are primarily attributed to the dissolution of metal ions into the DES forming complex as a result of which the values of density, refractive index and viscosity get increased. Conductivity exhibited a sharp rise after leaching due to the release of a larger number of ionic species. The dissolution behavior can be explained by proton-exchange and complexation mechanisms, Li^+ ions are readily released through substitution with H^+ of the lactic acid, accounting their efficient recovery. Co and Ni also dissolve completely because of their favorable interactions with COO^- and OH groups of DES. In contrast, Mn remains largely undissolved due to its higher stability and lower affinity for complexation. The FTIR spectra of leachate (Fig. 15) provides insight into the complexation occurring during the dissolution of cathode material when treated with Pro : LA (1 : 1) + 30% H_2O. The spectra revealed that the OH stretching vibration at 3383.5 cm^{-1} shifted to 3341.07 cm^{-1}. This shift was accompanied by a reduction in peak intensity and broadening of the band. Such behavior

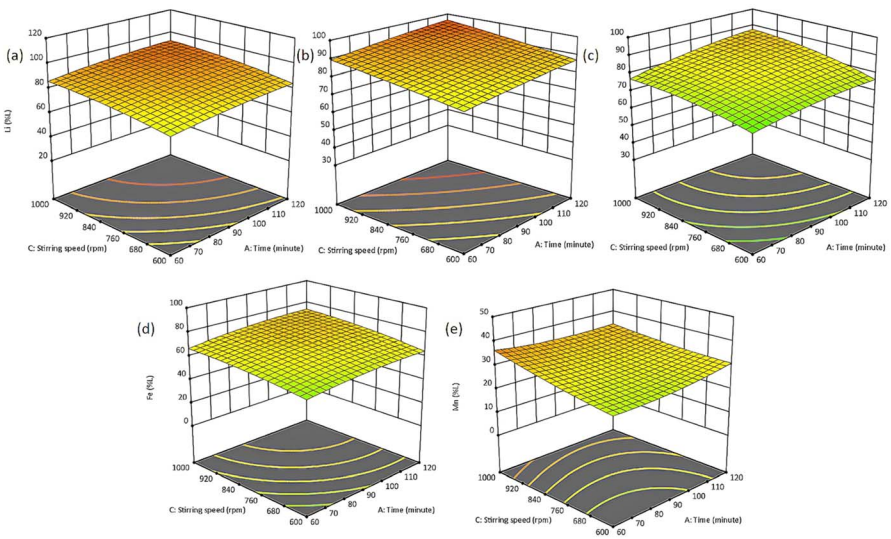

Fig. 13 Response surface plot showing the effect of stirring speed and time on the leaching efficiency of (a) Li, (b) Co, (c) Ni, (d) Fe, and (e) Mn.

Open Access Article. Published on 27 February 2026. Downloaded on 5/24/2026 11:28:39 AM. This article is licensed under a Creative Commons Attribution-NonCommercial 3.0 Unported Licence.

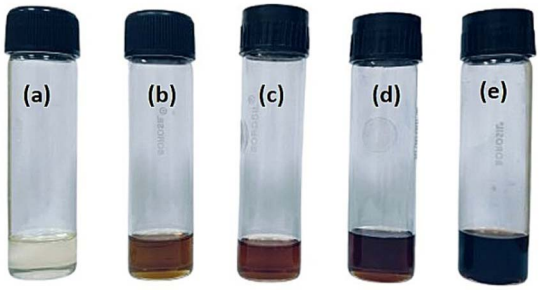

Fig. 14 Photographs of Pro : LA (1 : 1) + 30% H_2O (a) before leaching and cathode leachate (b) 30 minutes (c) 45 minute (d) 60 minutes, and (e) 120 minutes at 353 K.

reflects the strong metal oxide dissolution, where the hydrogen bond donors disrupt the metal–oxygen bonds in the LIB waste cathode material and facilitate metal extraction. The N–H stretching vibration was shifted from 3239.82 cm^{-1} to 3148.22 cm^{-1}. The shifting of N–H stretching vibration confirms the involvement of the DES functional groups in coordinating or interacting with dissolved metal ions. Peak observed at 1608.34 cm^{-1} for the C=O group in the Pro : LA (1 : 1) + 30% H_2O DES shifted to 1604.48 cm^{-1} after leaching. The COO stretching frequency also shifted from 1397.17 cm^{-1} to 1404.89 cm^{-1}. The CO stretching vibration peak changed from 1127.19 cm^{-1} to 1128.15 cm^{-1} after leaching. Shifts in these characteristic peaks compared to the DES system before leaching suggest reaction between metal ions (Li, Co, Ni, Fe, and Mn) and the DES. Mechanistically, the leaching process begins with the replacement of Li^+ ions by H^+ from the DES due to their high chemical reactivity, enabling preferential lithium extraction. Simultaneously, the –COOH group of lactic acid, known for its reducing nature, participates actively in the dissolution of transition-metal oxides. During this redox process, Co, Ni and Fe are reduced from their higher oxidation

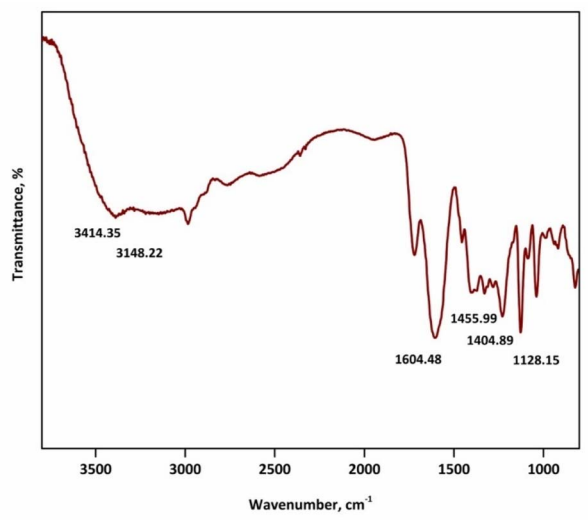

Fig. 15 FTIR spectra of cathode leachate after treating with Pro : LA (1 : 1) + 30% H_2O DES.

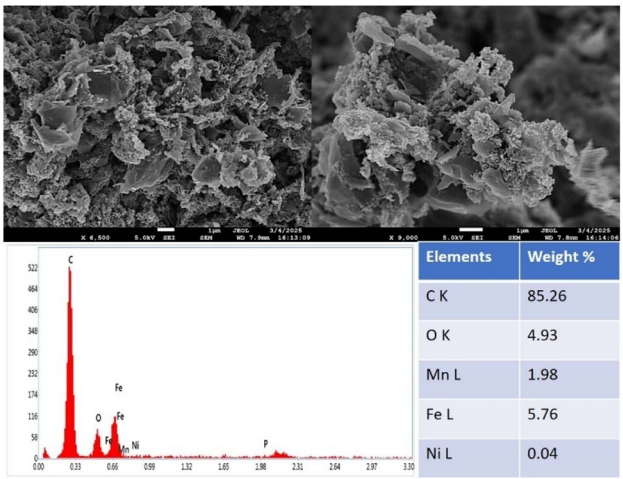

Elements	Weight %
C K	85.26
O K	4.93
Mn L	1.98
Fe L	5.76
Ni L	0.04

Fig. 16 SEM-EDX and elemental composition of the solid residue obtained after leaching.

states while the –COOH group undergoes dissociation releasing hydrogen ion, contributing to the observed decrease in O–H peak intensity. Overall, the FTIR results substantiate the formation of DES-metal complexes and validate that metal extraction proceeds through a combined mechanism of proton exchange, complexation, and redox reactions.

The solid residue obtained after leaching with Pro : LA (1 : 1) + 30% H_2O was subjected to morphological and characterization using SEM EDS. Fig. 16 presents the SEM-EDS characterization of leaching residues and as shown in this figure, leaching residue mainly exhibits agglomerated features, with an irregular shape and a rough surface. Through EDS analysis, it was found that the leaching residues chiefly consist of elements such as Fe, Mn, C, O with traces of Ni which is in accordance with the leaching profile. The XRD patterns of the solid residue after leaching are shown in Fig. 17. In the mixed cathode material, the diffraction peaks corresponding to layered oxide phases and $LiFePO_4$ are clearly observed, confirming the multiphase nature of the feed material. Especially, the characteristic peaks associated with $Li_2CoMn_3O_8$ are no longer detected in the residue, indicating the effective breakdown of this phase during leaching. The disappearance of these reflections may be attributed to the complete dissolution of cobalt containing phases, suggesting a preferential and efficient extraction of Co into the DES-water system. In contrast, the persistence of diffraction peaks indexed to $LiFePO_4$ and residual Mn/Fe-containing phases implies their partial stability under the applied leaching conditions.

The UV-visible spectrum of the cathode leachate exhibited distinct absorption bands corresponding to the d–d transitions of the dissolved transition metal ions, as shown in the Fig. 18. The absorption peaks observed at 333.59 nm and 719.9 nm are due to the $^3A_{2g}$ (F) → to $^3T_{1g}$ (P) transition corresponding to the octahedral complex of Ni^{2+}.[45] The distinct peak observed at 650.62 nm is characteristic of a tetrahedral Co^{2+} complex, suggesting that during the leaching process, due to coordination with the donor sites of the DES components tetrahedral cobalt complex is formed and it has been observed that leachate is

© 2026 The Author(s). Published by the Royal Society of Chemistry

Open Access Article. Published on 27 February 2026. Downloaded on 5/24/2026 11:28:39 AM.
This article is licensed under a Creative Commons Attribution-NonCommercial 3.0 Unported Licence.

blue in color. The weaker peak at 531.6 nm corresponds to Fe^{2+} complex because of charge transfer from DES to Fe^{2+}.[46]

A comparison of the leaching performance of this work with previously reported studies is presented in Table 5. The analysis compares our DES-based leaching process with conventional acid-based methods reported in the referenced works. While comparable or superior metal recovery efficiencies were achieved in this work (98.32% Li, 100% Co, 99.07% Ni, 85.63% Fe), our method operates under milder and safer conditions without strong mineral acids. This reduces the generation of hazardous acidic effluents, minimizes corrosion-related material costs, and decreases the need for extensive wastewater treatment, an important environmental concern noted in previous assessments of wet-chemical recycling processes. The economic evaluation also shows that the process benefits from low-cost, recyclable DES components and avoids the use of costly oxidants such as H_2O_2, improving its overall cost-effectiveness.

The recyclability of the Pro : LA (1 : 1) + 30% H_2O for leaching was checked by carrying out leaching cycles and adding precipitating agent (0.5 mol L^{-1} oxalic acid) to the metal-loaded DES solution. This causes the all Co, small amounts of Ni and Fe to form solid precipitates (*e.g.*, metal oxalates), which was then filtered out. The remaining DES was then reused for the second leaching cycle. It has been observed that after two cycles leaching efficiency for Co was decreased from 100 to 98.81% showing good recyclability option for Co Meanwhile, there was sharp decrease in the leaching efficiency of Li, Ni and Fe which is due to the presence of lots of these metals in the leachate (left after precipitation) after 1st leaching-precipitation cycle. Therefore, the recyclability test the Pro : LA (1 : 1) + 30% H_2O for separation of these metals will be validated in the extended part of our future work by using eco-friendly extractant *via* solvent extraction followed by selective precipitation.

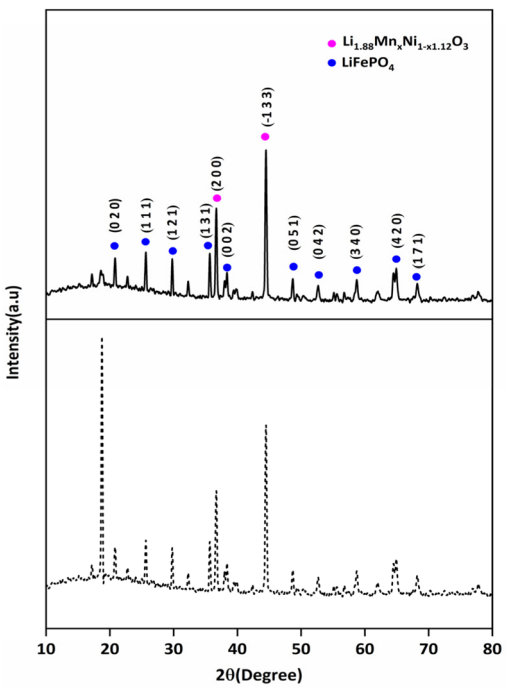

Fig. 17 XRD patterns of residue after leaching.

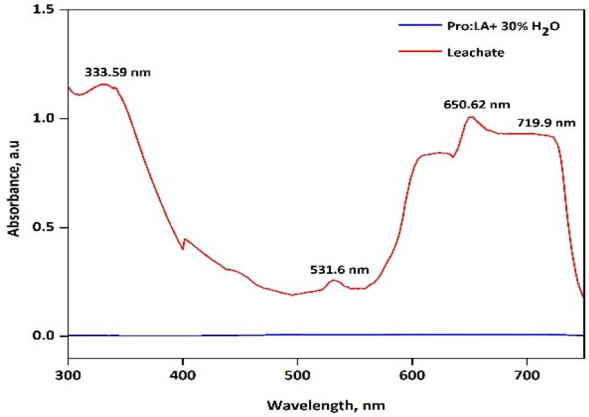

Fig. 18 UV-vis spectra of cathode leachate after treating with Pro : LA (1 : 1) + 30% H_2O DES under optimized conditions.

The leaching investigation of LIB waste cathode material using the Pro : LA (1 : 1) + 30% H_2O DES integrated with RSM-CCD optimization was specifically designed to address several core limitations of conventional LIB leaching processes, namely high acid consumption, use of corrosive reagents, poor selectivity, inefficient parameter tuning, and excessive energy demand. Traditional inorganic acid leaching usually requires high concentration of acids, elevated temperatures, use of harmful reducing agents and long leaching duration, often leading to non-selective dissolution of impurities as described in Table 5. In contrast, the present work employing Pro : LA (1 : 1) + 30% H_2O DES offers a mild, effective hydrogen-bonding and coordination environment, enabling higher metal dissolution. The application of RSM-CCD based systematic evaluation of the parameters such as temperature, leaching time, stirring speed and their interactive effects minimizes trial-and-error experimentation and identifies optimal operating conditions with reduced energy and solvent usage. Under optimized conditions of temperature 353 K, leaching time 120 minutes, and stirring speed of 900 rpm predicted by this model, leaching efficiencies of Li, Co, Ni and Fe were found as 98.32%, 100%, 99.07% and 85.63%, respectively. It demonstrates improved efficiency using eco-friendly Pro : LA (1 : 1) + 30% H_2O DES comparative to reported conventional leaching routes.

Leaching kinetics

Leaching reactions in metallurgical process are usually considered as heterogeneous, as they happen across multiple phases with well-defined boundaries between solids and liquids. Temperature, reaction duration, and system characteristics are very significant in influencing the leaching rate.[25,51] The principal reaction process involves the diffusion of the leaching agent from the bulk to the surface of cathode of LIB waste, where it chemically reacts with the positive electrode particles. The spherical solid particles steadily diminish as the reaction advances until they vanish entirely, and the resulting products along with leftover materials will create loose

Open Access Article. Published on 27 February 2026. Downloaded on 5/24/2026 11:28:39 AM. This article is licensed under a Creative Commons Attribution-NonCommercial 3.0 Unported Licence.

Table 5 Comparison of leaching efficiencies of the present work with reported studies from the literature

Source	Leaching condition	Leaching efficiency	Reference
Mixed LIB waste cathode	Pro : LA (1 : 1) + 30% H_2O DES, temperature 353 K, leaching time 120 minutes, and stirring speed of 900 rpm	98.32% Li, 100% Co, 99.07% Ni and, 85.63% Fe	This work
Spent $LiFePO_4$ batteries	Optimized conditions of leaching (0.8 mol $L^{-1}CH_3COOH$, 6 vol% H_2O_2, S/L ratio of 120 g L^{-1}, 50 °C, 30 min)	High leaching selectivity of around 94.08%	47
Spent LCO	1.5M $C_3H_6O_3$, 0.5 vol% H_2O_2, S/L ratio of 20 g L^{-1}, temperature 343 K and leaching time 20 minutes	98.9% Co, 98.5% Li	48
Mixed LIB waste cathode	2M $C_4H_6O_6$, 4 vol% H_2O_2, S/L ratio of 17 g L^{-1}, temperature 343 K and leaching time 30 minutes	99% of Li, Co, Mn, and Ni	49
Lithium iron phosphate (SLFP) and spent lithium manganate (SLMO)	Sulphuric acid concentration of 0.6 mol L^{-1}, temperature of 40 °C, a SLFP: SLMO molar ratio of 1, slurry density of 100 g L^{-1}, and reaction time of 120 min	Leaching efficiencies of Li and Mn reached as high as 99.99% and 70.02%	50

particles. Lastly the leached product is reverted to the bulk liquid through diffusion, which mostly comprises processes like diffusion and chemical reactions. To know about these in details, kinetic models such as shrinking-core, diffusion-based or surface chemical approaches are widely applied. These models allow identification of the rate-controlling step and thus clarify whether the process is chemically controlled, diffusion-controlled, or influenced by both mechanisms simultaneously.[52] Studying leaching kinetics not only provides insight into the mechanism of metal dissolution in DES but also helps to establish the rate controlling steps.[53] Such understanding is crucial for optimizing process efficiency and guiding the development of technically and economically viable leaching strategies. Among all variables, temperature has the strongest effect on leaching kinetics. Higher temperatures generally accelerate dissolution by lowering solvent viscosity, increasing the mobility of ions, and enhancing interfacial reactivity. The dissolution of cathode powder in the Pro : LA (1 : 1) + 30% H_2O DES follows a liquid–solid leaching pathway, where solid particles progressively diminish until complete dissolution occurs. When the overall process is limited by diffusion through the bulk solution, the rate equation is given as (eqn (7)):

$$1 - \frac{2}{3}x - (1 - x)^{2/3} = kt \quad (7)$$

When the chemical reaction is the rate determining step, the following reaction applies (eqn (8)):

$$1 - (1 - x)^{1/3} = kt \quad (8)$$

The fitting of the experimental data obtained under optimized conditions using the chemical reaction model exhibited an excellent fitting, as illustrated in Fig. 19. The chemical reaction is often a rate-controlling step, where the valuable metal is converted into a soluble product that moves into the bulk solution.

The specific rate constants obtained from the kinetic plots and temperature were plotted as given by the Arrhenius equation (eqn (9)).

$$\ln k = \ln A - \frac{E_a}{RT} \quad (9)$$

In this expression, k represents the specific rate constant, A represents the frequency factor, E_a the activation energy, R is the universal gas constant (8.314 $Jmol^{-1}K^{-1}$), and T is the temperature in Kelvin. The activation energy calculation was done using Arrhenius equation and the plot of ln K *versus* $1000/T$ has been included as Fig. S1 in SI. The resulted activation energies were found to be different for each metal, confirming chemically controlled leaching with metal-specific energy barriers. The existence of an oxygen-accepting constituent in DES most often the HBD is vital for cleavage of metal–oxygen bonds, which organizes the primary stage in oxide dissolution.[54] Lithium exhibits activation energy (22.45 kJ mol^{-1}), reflecting its relatively weak Li–O ionic bonding and low lattice energy, which facilitates rapid proton exchange. Iron shows the lowest activation energy (13.52 kJ mol^{-1}), indicating comparatively facile dissolution, which can be attributed to the vulnerability of Fe–O bonds to proton-assisted cleavage and reduction under acidic DES conditions. In contrast, cobalt displays the highest activation energy (38.32 kJ mol^{-1}), consistent with the stronger Co–O bond strength and higher lattice stabilization in layered oxide structures, requiring greater energy input for bond disruption and redox transformation. Nickel shows activation energy of 25.37 kJ mol^{-1}. Habashi[55] reported that the activation energy between 4.2 kJ mol^{-1} and 13 kJ mol^{-1} demonstrates the diffusion control reaction. Moreover, the activation energy between 13 kJ mol^{-1} and 42 kJ mol^{-1} reflects a mixed control reaction. In the present study the observed values of activation energy (more than 13 kJ mol^{-1}) ensures the mixed control regime (diffusion as well as chemical reaction) for leaching of all metals. Since the

© 2026 The Author(s). Published by the Royal Society of Chemistry

Open Access Article. Published on 27 February 2026. Downloaded on 5/24/2026 11:28:39 AM.
This article is licensed under a Creative Commons Attribution-NonCommercial 3.0 Unported Licence.

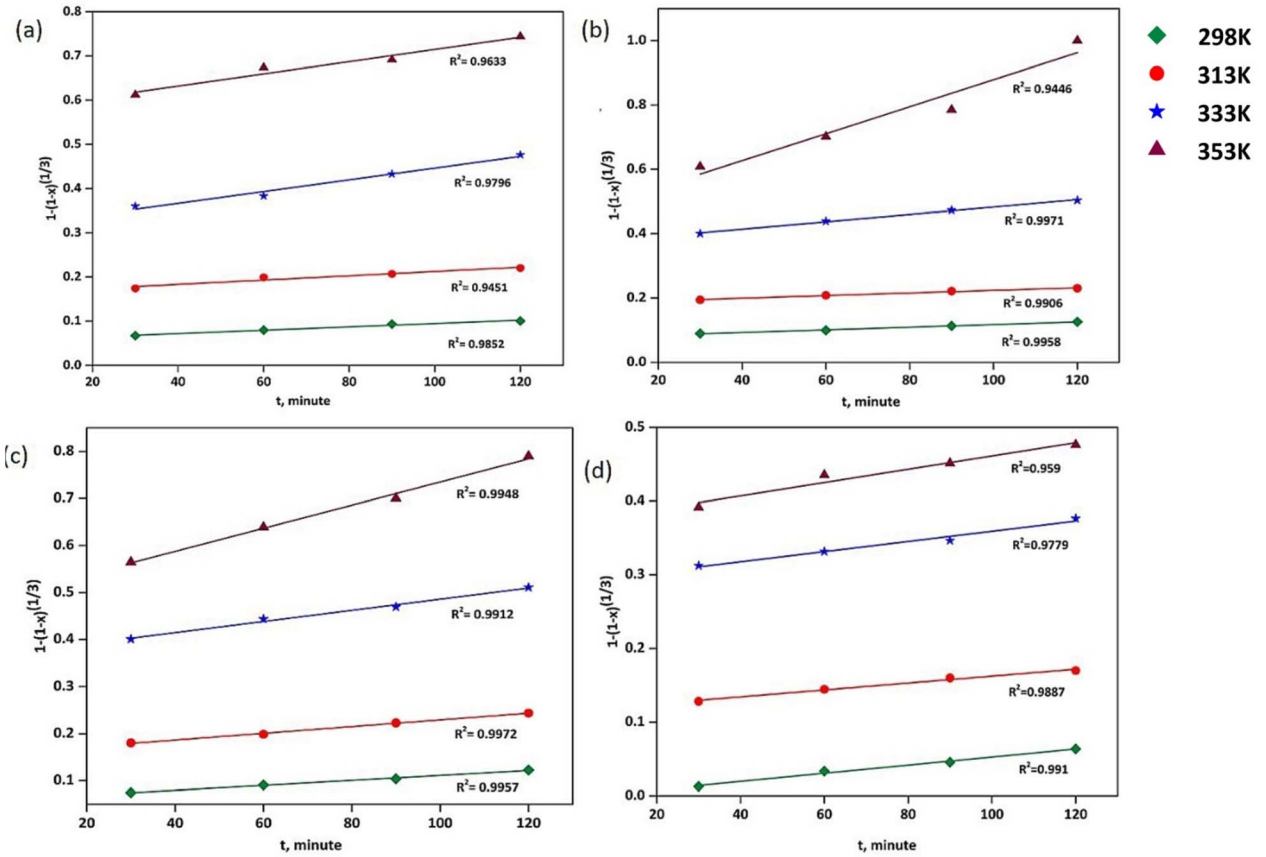

Fig. 19 Reaction control kinetic plots showing the linear fitting of leaching data for (a) Li, (b) Co, (c) Ni, and (d) Fe in Pro : LA (1 : 1) + 30% H_2O DES at different temperature.

experiments were executed under high stirring speed conditions at 900 rpm, the effect of diffusion may be neglected.[53]

Conclusions

In this work, Pro : LA (1 : 1) + 30% H_2O was successfully synthesized and characterized for the sustainable leaching of Li, Co, Ni, Fe, and Mn from mixed spent LIBs cathode powder. The thermo physical properties of the DES-water system, including density, refractive index, viscosity, and conductivity at different temperature (298 K to 323 K), were systematically evaluated, and the effect of water addition (10–40%) on its H-bonding network was confirmed through FTIR spectroscopy. Under optimized conditions of temperature 353 K, leaching time 120 minutes, and stirring speed of 900 rpm the system achieved 98.32% Li, 100% Co, 99.07% Ni, and 85.63% Fe recovery, demonstrating its strong capability for efficient metal dissolution. The elevated temperature, time and stirring speed promotes intrinsic kinetics and external mass transfer which enable nearly complete dissolution of Li, Co and Ni. In contrast, Fe shows a relatively lower but substantial recovery. The comparatively low Mn recovery is consistent with the slower dissolution of higher-valence Mn species; in the absence of strong reductant, Mn^{3+}/Mn^{4+} phases are less readily converted to soluble Mn^{2+}, making Mn leaching kinetically and thermodynamically least favorable. This work establishes the potential of amino acid-based DES for green hydrometallurgical process and paves the way for future scale-up in LIBs battery recycling. It highlights the designing of DESs with low viscosity, strong coordination, and high ability for optimal dissolution along with environmentally friendly recycling approach. Compared with choline chloride-based DES, L-proline–lactic acid DES exhibits lower preparation cost, superior biodegradability, and does not require high-temperature conditions during synthesis, which further highlights its green and sustainable characteristics and broad application potential in the field of hydrometallurgy for spent lithium-ion batteries. The difficulties and possibilities associated with improving valuable metal recovery through DESs are crucial for creating a blueprint for pioneering uses of DES technology.

Author contributions

Pratyasha Panda: investigation, visualization, writing – original draft, data curation, methodology, software. Sujata Mishra: conceptualization, writing – review & editing, supervision.

Conflicts of interest

There is no conflicts of interest to declare.

© 2026 The Author(s). Published by the Royal Society of Chemistry

Open Access Article. Published on 27 February 2026. Downloaded on 5/24/2026 11:28:39 AM. This article is licensed under a Creative Commons Attribution-NonCommercial 3.0 Unported Licence.

Data availability

The data supporting this article have been included as part of the main document and will be available on request.

Supplementary information (SI): provides statistical significance of model terms evaluated by using RSM-CCD optimization as well as the Arrhenius plots for leaching kinetics. See DOI: https://doi.org/10.1039/d5ra09345g.

Acknowledgements

The authors sincerely acknowledge Siksha 'O' Anusandhan (Deemed to be University) for providing the necessary facilities and support. P. Panda is grateful to A. R. Ray for his kind help and suggestions.

References

1 Z. A. Sandhu, B. Iqbal, M. A. Raza, N. Kainat, S. Ashraf, U. Farwa, A. Ashraf, A. Arishi and T. Rasheed, *Chem. – Asian J.*, 2025, **20**(16), e00299, DOI: 10.1002/asia.202500299.
2 O. Ahmadzadeh, R. Rodriguez, J. Getz, S. Panneerselvam and D. Soudbakhsh, *Environ. Impact Assess. Rev.*, 2024, **110**, 107668.
3 Z. Liu, F. Feng, W. Feng, G. Wang, B. Qi, M. Gong, F. Zhang and H. Pang, *Energy Environ. Sci.*, 2025, **18**(8), 3568–3613.
4 S. Link, L. Schneider, A. Stephan, L. Weymann and P. Plötz, *Nat. Energy*, 2025, **10**, 526–534.
5 N. Kumar, A. Mishra and D. Kumar, *Miner. Eng.*, 2025, **227**, 109312.
6 J. H. Suh, H. Lee, J. Kim, H. Bae, J. H. Shim, W. K. Pang, Y. H. Kim, S. Kim, J. Mun, T. Song and J. H. Kim, *Carbon Neutralization*, 2025, **4**(4), e7001, DOI: 10.1002/cnl2.70018.
7 M. Rinne, H. Lappalainen and M. Lundström, *Green Chem.*, 2025, **27**(9), 2522–2537.
8 S. Paul and P. Shrotriya, *Materials*, 2025, **18**, 613.
9 P. Panda and S. Mishra, *J. Mol. Liq.*, 2023, **390**, 123070.
10 J. Płotka-Wasylka, M. De La Guardia, V. Andruch and M. Vilková, *Microchem. J.*, 2020, **159**, 105539.
11 C. Li, J. Jin, Z. Yuan, C. Zhang, L. Wu and C. Wang, *ChemistryOpen*, 2025, **14**(4), e202400258, DOI: 10.1002/open.202400258.
12 H. Zou, E. Gratz, D. Apelian and Y. Wang, *Green Chem.*, 2013, **15**, 1183.
13 S. Li, W. Zhang, Y. Xia and Q. Li, *Waste Manage.*, 2024, **189**, 23–33.
14 L. M. J. Rouquette, M. Petranikova and N. Vieceli, *Sep. Purif. Technol.*, 2023, **320**, 124143.
15 A. Porvali, M. Aaltonen, S. Ojanen, O. Velazquez-Martinez, E. Eronen, F. Liu, B. P. Wilson, R. Serna-Guerrero and M. Lundström, *Resour., Conserv. Recycl.*, 2018, **142**, 257–266.
16 X. Chen, C. Guo, H. Ma, J. Li, T. Zhou, L. Cao and D. Kang, *Waste Manage.*, 2018, **75**, 459–468.
17 D. Song, T. Wang, Z. Liu, S. Zhao, J. Quan, G. Li, H. Zhu, J. Huang and W. He, *J. Environ. Chem. Eng.*, 2021, **10**, 107102.
18 H. Chu, J. Lie and J.-C. Liu, *J. Sustain. Metall.*, 2021, **7**, 630–641.
19 J. Wu, L. Xiao, L. Shen, J.-J. Ran, H. Zhong, Y.-R. Zhu and H. Chen, *Rare Met.*, 2023, **43**, 879–899.
20 S. H. Alhashim, S. Bhattacharyya, R. Tromer, A. Kabbani, G. Babu, E. F. Oliveira, D. S. Galvao and P. M. Ajayan, *ACS Sustain. Chem. Eng.*, 2023, **11**, 6914–6922.
21 M. Jafari, S. Z. Shafaie, H. Abdollahi and A. Entezari-Zarandi, *J. Environ. Chem. Eng.*, 2022, **10**, 109014.
22 S. Tang, M. Zhang and M. Guo, *ACS Sustain. Chem. Eng.*, 2022, **10**, 975–985.
23 Q. Yan, A. Ding, M. Li, C. Liu and C. Xiao, *Energy Fuels*, 2023, **37**, 1216–1224.
24 P. Yang, L. Zhou, J. Zeng, Y. Ye, J. Lan, X. Xie, Y. Chen, X. Wang and R. Ao, *J. Environ. Chem. Eng.*, 2025, **14**, 120726.
25 M. Cheng, J. Ru, Q. Zhang, Y. Hua, C. Xu, Y. Zhang and D. Wang, *ACS Sustain. Chem. Eng.*, 2025, **13**, 1719–1728.
26 B. Parraguez, M. J. Inestrosa-Izurieta and J. I. Urzúa, *Process Saf. Environ. Prot.*, 2025, **219**, 296–305.
27 S. Karimi, L. Mafton-Azad, B. Behnajady and B. Tüzün, *Korean J. Chem. Eng.*, 2025, **42**(2), 31–381.
28 Z. Chu, B. Zhao, Y. Chen, S. Hu, J. Li and K. Liu, *J. Power Sources*, 2025, **641**, 236886.
29 I. Mansinhos, S. Gonçalves, R. Rodríguez-Solana, J. L. Ordóñez-Díaz, J. M. Moreno-Rojas and A. Romano, *Antioxidants*, 2021, **10**, 582.
30 N. Peeters, K. Binnemans and S. Riaño, *Green Chem.*, 2020, **22**, 4210–4221.
31 O. S. Hammond, D. T. Bowron, A. J. Jackson, T. Arnold, A. Sanchez-Fernandez, N. Tsapatsaris, V. G. Sakai and K. J. Edler, *J. Phys. Chem. B*, 2017, **121**, 7473–7483.
32 O. S. Hammond, D. T. Bowron and K. J. Edler, *Angew. Chem., Int. Ed.*, 2017, **56**, 9782–9785.
33 S. Maharana, R. R. Maharana, K. Samanta and S. Mishra, *ACS Omega*, 2025, **10**(32), 36041–36055, DOI: 10.1021/acsomega.5c03618.
34 H. Shirota, M. Koyakkat, J. Rajbangshi and R. Biswas, *J. Phys. Chem. B*, 2025, **129**(3), 965–978.
35 R. B. Leron, A. N. Soriano and M. H. Li, *J. Taiwan Inst. Chem. Eng.*, 2012, **43**, 551–557.
36 P. Panda and S. Mishra, *Environ. Res.*, 2025, **269**, 120917.
37 A. Yadav and S. Pandey, *J. Chem. Eng. Data*, 2014, **59**, 2221–2229.
38 R. Craveiro, I. Aroso, V. Flammia, T. Carvalho, M. T. Viciosa, M. Dionísio, S. Barreiros, R. L. Reis, A. R. C. Duarte and A. Paiva, *J. Mol. Liq.*, 2016, **215**, 534–540.
39 M. Aroso, A. Paiva, R. L. Reis and A. R. C. Duarte, *J. Mol. Liq.*, 2017, **241**, 654–661.
40 A. Gutiérrez, M. Atilhan and S. Aparicio, *J. Mol. Liq.*, 2021, **339**, 116758.
41 S. S. Behera and P. K. Parhi, *Sep. Purif. Technol.*, 2016, **160**, 59–66.
42 V. Athanasiadis, D. Palaiogiannis, K. Poulianiti, E. Bozinou, S. I. Lalas and D. P. Makris, *Sustainability*, 2022, **14**, 6864.
43 M. Pazara, G. Provelengiadi, M. Mantiniotou, V. Athanasiadis, I. Samanidis, I. Makrygiannis, I. F. Tzavellas, I. C. Martakos, N. S. Thomaidis and S. I. Lalas, *Processes*, 2025, **13**, 2283.

© 2026 The Author(s). Published by the Royal Society of Chemistry

Open Access Article. Published on 27 February 2026. Downloaded on 5/24/2026 11:28:39 AM.
This article is licensed under a Creative Commons Attribution-NonCommercial 3.0 Unported Licence.

44 T. Nshizirungu, M. Rana, Y. T. Jo, E. Uwiragiye, J. Kim and J.-H. Park, *J. Environ. Chem. Eng.*, 2024, **12**, 112371.
45 H. Bastos, N. Schaeffer, J. M. Pringle, M. Eftekharnia, J. A. P. Coutinho and C. Pozo-Gonzalo, *Sep. Purif. Technol.*, 2025, **364**, 132354.
46 S. Karampelas, L. Kiefert, D. Bersani and P. Vandenabeele, *Gems Gemol.*, 2020, DOI: 10.15506/JOG.2020.37.4.434.
47 Y. Yang, X. Meng, H. Cao, X. Lin, C. Liu, Y. Sun, Y. Zhang and Z. Sun, *Green Chem.*, 2018, **20**, 3121–3133.
48 L. Li, E. Fan, Y. Guan, X. Zhang, Q. Xue, L. Wei, F. Wu and R. Chen, *ACS Sustain. Chem. Eng.*, 2017, **5**, 5224–5233.
49 L.-P. He, S.-Y. Sun, Y.-Y. Mu, X.-F. Song and J.-G. Yu, *ACS Sustain. Chem. Eng.*, 2016, **5**, 714–721.
50 Z. Zhang, R. Lu, T. Li, Z. Liu, H. Nie, R. Wang, Z. Xu and K. Yan, *Green Chem.*, 2025, **27**(17), 4688–4705.
51 T. Ketegenov, K. Kamunur, L. Mussapyrova, A. Batkal and R. Nadirov, *Metals*, 2024, **14**, 1052.
52 M. Jafari, S. Z. Shafaie, H. Abdollahi and A. Entezari-Zarandi, *Miner. Process. Extr. Metall. Rev.*, 2022, **44**, 218–230.
53 B. Chenthamara and R. L. Gardas, *ACS Sustain. Chem. Eng.*, 2024, **12**, 12827–12836.
54 H. M. Khalid and R. M. Santos, *Hydrometallurgy*, 2025, **238**, 106571.
55 F. Habashi, *Principles of Extractive Metallurgy*, General principles, Gordon and Breach, New York, 1969, vol. 1.